ALIGNMENT OF CdSe/CdS NANOPARTICLES IN UV-CURABLE RESIN FOR APPLICATIONS IN LUMINESCENT SOLAR CONCENTRATORS

A Thesis

by

NICHOLAS JAMES GRIPP

Submitted to the Office of Graduate and Professional Studies of
Texas A&M University
in partial fulfillment of the requirements for the degree of

MASTER OF SCIENCE

Chair of Committee,	Matthew Sheldon
Committee Members,	Jaime Grunlan
	Svetlana Sukhishvili
Head of Department,	Ibrahim Karaman

August 2019

Major Subject: Materials Science and Engineering

ABSTRACT

Highly luminescent UV-curable nanocomposites with parallel alignment of colloidal nanorods possessing dipolar emission are desired for applications in luminescent solar concentrators. Here, we show that full alignment of colloidal CdSe/CdS core-shell nanorods can be achieved in solution using external AC electric fields. Partial alignment of nanorods is achieved in resin using this same method. Nanorod orientation is determined by measuring the concurrent change in absorbance as a function of an applied electric field. In addition, we show that highly fluorescent optical quality nanocomposites with monodisperse nanorods can be produced using a UV-curable resin. Ordered nanocomposites are produced by curing the resin while the films are under an applied electric field. An ultra-microtome is used to probe nanorod orientation within the cured nanocomposite via TEM imaging to calculate an order parameter that quantifies the degree of alignment present in the films.

ACKNOWLEDGEMENTS

I would like to thank my committee chair, Dr. Sheldon, and my committee members, Dr. Grunlan and Dr. Sukhishvili for their guidance and support during my time here at Texas A&M. I am especially grateful for the encouraging atmosphere that Dr. Sheldon has created in his research group. It made the struggle and problems encountered during this research enjoyable.

I would like to thank my friends, colleagues, and the Department of Chemistry and Material Science and Engineering faculty and staff for being so helpful and accepting during my time here at Texas A&M University. I am going to miss being a member of the Sheldon Research Group and all that comes along with it. Every member of the team has on multiple occasions gone out of their way to help me accomplish my goals. Specifically, I would like to thank Rivi Ratnaweera for being such a valuable research partner. We have accomplished so much during our time together and it will always be a pleasant memory. I would like to thank Benjamin Roman and Je-Ruei Wen for their help with taking TEM images and general laboratory instruction. I would like to thank Richard Littleton for his instruction and work on sample preparation using the ultramicrotome.

I want to thank the Gordon and Betty Moore Foundation for providing the funding that allowed me to complete my research project.

Finally, I would like to thank my parents for doing so much to support me during my time as a student. Without their guidance and support I would not be where I am today.

CONTRIBUTORS AND FUNDING SOURCES

Contributors

This work was supervised by a thesis committee consisting of Professor Matthew Sheldon and Professor Svetlana Sukhishvili of the Department of Materials Science and Engineering and Professor Jaime Grunlan of the Department of Mechanical Engineering. All work was conducted for the thesis was completed by the student independently.

Funding Sources

This work was made possible in part by the Gordon and Betty Moore Foundation under Grant Number GBMF6882.

NOMENCLATURE

LSC	Luminescent Solar Concentrator
UV	Ultraviolet
UV-Vis	Ultraviolet – Visible Spectrum
TEM	Transmission Electron Microscopy
XRD	X-ray Diffraction
CdSe	Cadmium Selenide
CdS	Cadmium Sulfide
NR	Nanorods
PLQY	Photoluminescent Luminescent Quantum Yield
LMA	Lauryl Methacrylate
EGDM	Ethylene Glycol Dimethacrylate
ITO	Indium Tin Oxide

TABLE OF CONTENTS

PAGE

LIST OF FIGURES

PAGE

LIST OF EQUATIONS

PAGE

CHAPTER I

INTRODUCTION

As the need for clean energy increases, the focus shifts evermore to the development of renewable energy technologies that will be economically viable sources of global energy. One such avenue is harnessing solar energy via photovoltaic (PV) materials. The efficiencies of solar cells have continued to rise to values upwards of 46% in thanks to cell design and the introduction of highly engineered materials into the devices.[1] The figure of merit for solar cells is the power conversion efficiency, a measure of the output electrical power created by a known amount of incident light power. While the efficiencies of such cells are quite high, applications are limited by the production costs and material availability. Ideally, a device design that could maximize the amount of incident light power and minimize the photovoltaic material needed would allow for cheaper clean energy to be produced. Some of the most popular device configurations for improving efficiency focus on expanding the accessible spectrum using multi-junction or mixed bandgap cells. Another area of research aims to more effectively harness the incident light that is entering or leaving the cell by enhancing light trapping.

One promising approach to reducing the cost and expanding the global applications of solar energy is the use of luminescent solar concentrators (LSCs). A typical LSC design is composed of a plastic waveguide with embedded luminescent dyes and PV material around the edges of the device. The plastic waveguide and dye are responsible for collecting the incident light and then, using isotropic emission and total internal reflection direct the photons towards the solar cell for absorption. There are some loses associated with this design that limit its commercial applicability. A major loss occurs when the light emitted by the fluorophore is not

internally reflected and instead, leaves the waveguide through an escape cone.[2] Reabsorption by a neighboring fluorophore is another common loss pathway: the photon is often lost due to thermalization and does not make it to the PV material. Light can also be scattered or pass through the waveguide due to incompatible absorption bands.[2]

A proposed method of reducing the loses associated with LSCs devices is the application of a waveguide featuring aligned fluorophores. Using anisotropic nanoparticles instead of quantum dots or luminescent dyes allows for the particles to have a preferential emission axis that, when combined with the proper device fabrication, can boost the LSC performance. The implementation of aligned particles is thought to attenuate the surface losses due to emission through the escape cone to less than 10%.[3-4] In addition to reduced surface losses, the aligned fluorophores can increase the energy that makes it to the PV material by more than 30%.[5]

The cadmium selenide/cadmium sulfide (CdSe/CdS) dot-in-rod heterostructures have been a common material investigated for solar applications in recent years. Their tunable aspect ratio and core size allow for controlled emission with high photoluminescence quantum yield (PLQY).[6] The dot-in-rod morphology gives rise to anisotropic emission which can be used to improve efficiency in photovoltaic systems.[7] CdSe/CdS NRs strongly absorb and emit light polarized parallel to their long axis.[8] The large bandgap CdS shell absorbs photons and transfers energy to the smaller band gap CdSe core giving rise to Stokes-shifted emission. The Stokes shift is important in LSC applications in order to reduce reabsorption losses.[9]

Alignment of colloidal NRs can be achieved using a number of methods. Self-assembly during solvent drying is a common way to achieve alignment of the NRs with their long axis parallel to a substrate surface. Other liquid phase evaporation treatments have been shown to align the particles perpendicular to the substrate surface.[10-15] Another avenue of alignment

involves an external force, either mechanical or an applied field to induce alignment of colloidal NRs.[16] Here, we utilize an applied electric field to reach full alignment of NRs in solution (dodecane) and to produce resin nanocomposites embedded with ordered NRs. As mentioned beforehand, an LSC with alignment fluorophores will guide more energy to the PV material and achieve have a higher efficiency than those with isotropic emitting fluorophores.[5]

The aim of this research is to understand the fundamentals associated with aligning CdSe/CdS dot-in-rod heterostructures with anisotropic dipole emission in a UV-curable resin. A result of optimizing this production process will be the production of ordered nanocomposite thin films that can be utilized in luminescent solar concentrators. The term “ordered” would be attributed to the relative alignment of the nanoparticles contained within the resin matrix. After producing ordered thin films, the next step is to quantify the degree of alignment present in the sample. There are two proposed methods for this: taking thin slices (30-250 nm) of nanocomposite using an ultra-microtome and imaging them using transmission electron microscopy (TEM) or by measuring the fluorescence anisotropy of the resin films. For both methods we develop an order parameter indicative of the degree of alignment present in the films.

CHAPTER II

METHODOLOGY

Synthesis and Characterization of CdSe/CdS Heterostructures

The cadmium selenide quantum dots (CdSe QDs) and the cadmium selenide/cadmium sulfide dot-in-rod heterostructures (CdSe/CdS NRs) were both synthesized using a hot injection reaction. Our synthesis procedure was modeled based on the work done by Carbone and Nobile.[17] All chemicals and solvents were purchased from Sigma-Aldrich.

The CdSe QDs were synthesized, cleaned, and characterized prior to use in the synthesis of the heterostructures. In a round-bottom flask, cadmium oxide (CdO), trioctylphosphine oxide (TOPO), and octadecylphosphonic acid (ODPA) are heated to 150 °C for 1.5 h under vacuum to remove all moisture and oxygen. The flask is purged with argon and heated to 300 °C where trioctylphosphine is added, the solution is heated until clear. Upon turning clear, the flask is heated to 350 °C where a solution of TOP and selenium (Se) is added. Depending on the desired particle diameter, the flask is held at 350 °C for 0-6 minutes before removing from the heat. In our synthesis the flask is left at 350 °C for 90 seconds before being cooled.

The cleaning process involves dropping the quantum dots out of solution (toluene and TOP) using methanol. Methanol is added dropwise until the solution becomes cloudy, where it is centrifuged at 3000 gs for 10 minutes. The centrifugation of the solution causes the nanoparticles, which have been destabilized and dropped out of solution, to collect at the bottom of the vial while the excess ligands remain solubilized in the supernatant. The supernatant is drained, and the dots are resolubilized in toluene. The ethanol addition is repeated and then centrifuged for a second time. This process is repeated until the solution no longer forms bubbles

when shaken, generally three times. The bubbles are a product of extra ligands in solution, which are essentially soaps. The quantum dots are then characterized using UV-Vis, XRD and TEM to ensure they have a monodispersed size distribution and the desired particle diameter is achieved.

After successfully synthesizing a monodispersed sample of quantum dots of the desired diameter, the "shelling" procedure may begin. During this hot-injection synthesis, a heterostructure is produced by growing a CdS layer that encapsulates the CdSe seed. This procedure is also adapted from Carbone and Nobile's publication, *Synthesis and micrometer-scale assembly of colloidal CdSe/CdS nanorods prepared by a seeded growth approach*.[17] They provide a detailed synthesis table of different aspect ratio heterostructures, and the required dot diameter and reaction conditions necessary for the production of such dot-in-rod morphologies.

In a round-bottom flask, CdO, TOPO, and hexylphosphonic acid (HPA) are heated at 150 °C for 1.5 h under vacuum to remove all moisture and oxygen. The flask is purged with argon and heated to 300° C where trioctylphosphine is added, the solution is heated until clear. Once clear, the flask is heated to the indicated reaction temperature (350 °C) where a solution of TOP, CdSe QDs, and sulfur (S) is added. The heat is maintained for the desired reaction time before cooling the solution.

Once synthesized, the heterostructures must be cleaned using the same method previously described. An unclean nanoparticle will have decreased photoluminescent quantum yield (PLQY) due to excess ligands on the surface. The nanoparticles should be characterized using UV-Vis spectroscopy, TEM imaging, and XRD to ensure the correct morphology.

Field Alignment of Nanorods

An AC electric field was used to align the NRs in solution. The degree of alignment was monitored by measuring concurrent changes in transmittance/absorbance. Figure 1 shows a schematic of the optimized experimental setup. A model GFG-3015 function generator (Gwinstek) and Model 2220 high-voltage amplifier (Trek) were used to apply a high voltage AC field across a sample cell containing a colloidal NR dispersion. During field alignment, the transmission of a blue (405 nm) laser was measured using a model 2007 Nirvana detector 125 kHz auto-balanced photoreceiver (New Focus). The time resolved input and response were visualized using a MSO2000A/DS2000A series oscilloscope (Rigol).

A free space 405 nm continuum laser (RGBLase) is used to ensure that the nanoparticles are excited by the beam. The laser is mounted on a heat sink in order to manage the temperature of the laser housing and allow for a constant laser power. The apertures and lenses used to focus the laser beam are from ThorLabs. The neutral density (ND) filter is used to control the power of light that reaches the detector to ensure that no damage or saturation occurs during testing. The oscilloscope also had an input signal from the function generator which displayed the waveform of the voltage applied to the sample. The model GFG-3015 function generator (Gwinstek) can generate a sinusoidal or square waveform with an amplitude of +/- 10V and a frequency range of 0.01 Hz-15 MHz. Prior to reaching the sample, the waveform passes through the Trek Model 2220 high voltage generator, the generator applies a gain of 153. The high voltage generator applies the voltage to the sample cell via two electrodes which allow for a field to be generated between them.

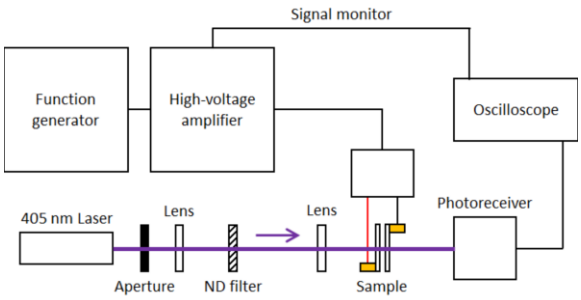

Figure 1: Schematic of alignment measurement optical set up

Originally, the cell was comprised of a thin capillary tube sandwiched by two copper electrodes. This design proved challenging as the curved edges of the capillary diffracted the beam and made getting a strong signal difficult. The cylindrical geometry did not allow a uniform electric field to be applied across the cell, producing an output signal with low signal-to-noise (S/N). As a solution, two pieces of Indium Tin Oxide (ITO) coated glass slides were implemented to reduce diffraction issues and create a more uniform electric field across the sample. The spacing between the ITO slides is controlled by a UV curable optics glue with embedded spacer beads. The spacers used in this experiment range from 50 µm to 1000 µm (Cospheric). As the size of the spacer beads decreased and the field strengths became higher, short circuiting became a common mode of failure in the ITO sample cells. Short circuiting caused the ITO film to burn and delaminate from the glass substrate, making the cell unusable. The location of the shorting is generally located away from the sample, in a region of air or glue. To remedy this problem, the full ITO slides were replaced by a templated ITO slide (MSE Supplies) shown in figure 2 & 3. This slide design ensures that the field is only applied to regions that contain sample.

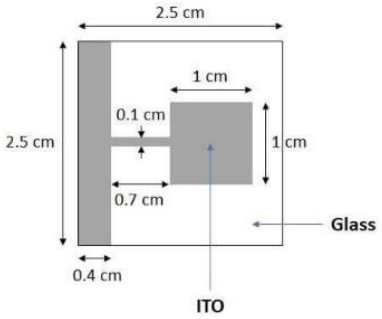

Figure 2: Patterned ITO slide template

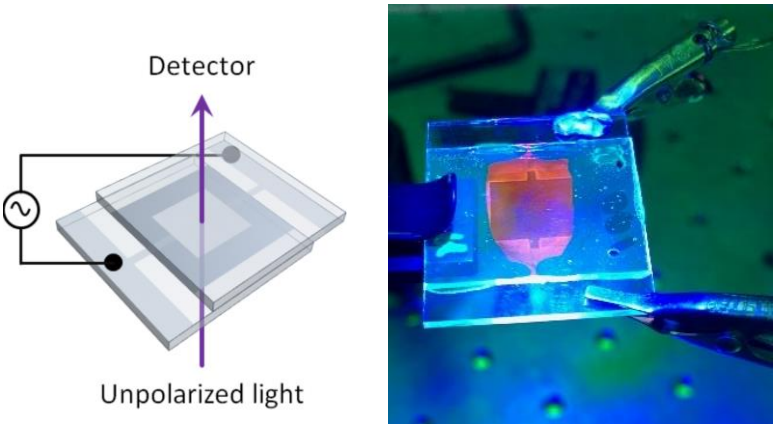

Figure 3: Image of sample cell schematic and fabricated cell filled with CdSe/CdS in dodecane

The addition of the templated ITO slides allowed for much higher field strengths to be achieved without shorting or cell damage. Prior to the templated cells, the breakdown field strength was approximately 8 V/µm. This value increased to 30.6 V/µm with the templated slides.

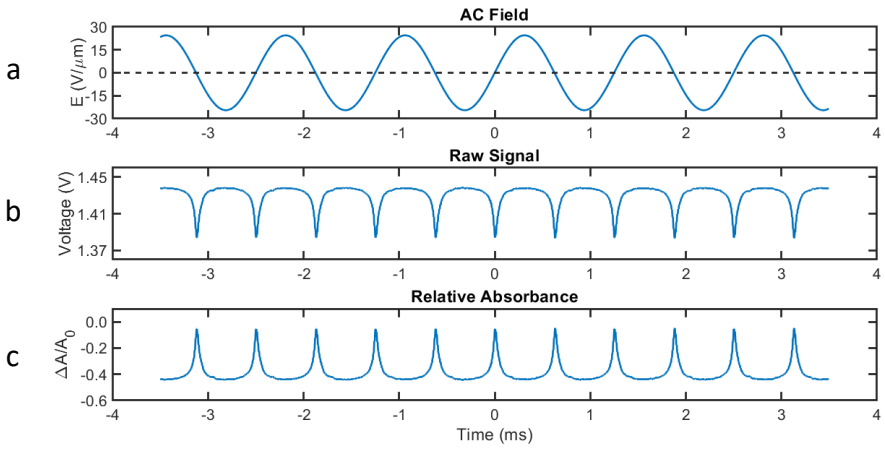

Figure 4: a) Applied electric field strength from function generator waveform amplified by high voltage amp. b) Photodiode response voltage. c) Relative absorbance as a function of the applied field.

The plots in figure 4a,b,c are an example of the data recorded during an alignment study. Plot 4a is the field strength due to the input signal created by the function generator and amplified by the high voltage amp. Typically, a sinusoidal function is used as it offers a smoother transition between the positive and negative fields compared to a square-wave or triangular wave-form, making it less susceptible to short-circuiting. Plot 4b is the output signal recorded by the oscilloscope corresponding to the transmitted light intensity as detected by the photoreceiver. When a positive electric field is applied, the NRs begin to orient themselves normal to the ITO plates. This causes an increase in the transmittance of the sample due to the long axes of the NRs being oriented perpendicular to the plane of polarization. This is reflected by the maxima in the output signal. As the field approaches zero, the NRs return to a random state, leading to a decrease in transmittance. This behavior is mimicked in the negative field region of the input function as the nanorods would still be aligned perpendicular to the plane of polarization. Variations in transmittance or absorbance can be used to monitor the degree of

dynamic alignment. However, these measurements would be sensitive to changes in concentration, film thickness, and laser power fluctuations, etc. To eliminate such external effects, the absorbance (A) can be normalized by the absorbance at zero field (A_0). This quantity is defined as the relative absorbance, shown in equation 1. Figure 4c shows the plot of relative absorbance as a function of the applied electric field.

$$\frac{\Delta A}{A_0} = \frac{A - A_0}{A_0} \quad (1)$$

Uv-Curable Resin Thin Films

The resin is composed of the monomer lauryl methacrylate (LMA) and cross-linking agent ethylene glycol dimethacrylate (EGDM), as well as a photo initiator (IRGA 819). Each of the components were purchased from Sigma-Aldrich. For the sake of chemical stability, the EGDM must be stored at low temperatures in an air-free environment. The three components should be stirred when mixed for a minimum of 1h to ensure that a homogenous mixture is formed. It is recommended that all mixing and storage should be done under an inert atmosphere, especially when mixing the NRs into the mixture. All curing is done using a Sun Spot 2 UV curing lamp (Uvitron).

Incorporating Nanorods Into Resin

It is imperative that the NRs be completely solubilized in the resin, if not, a monodispersed material cannot be produced. Prior to use in the resin samples, the nanorods must be removed from their storage solvent, hexanes. This is achieved by flowing nitrogen over the solution until a thick paste remains. The resin is added to the vial where the NRs are mixed with

the resin using ultra-sonication for 30 minutes. Ultrasonication ensures that no undesired aggregates form in the resin during curing.

Ultra-Microtome Slicing & TEM

TEM imaging is a valuable tool gain a direct understanding of how the NPs are behaving in the resin. In this study, a FEI Tecnai G2 F20 ST FE-TEM is used to obtain high quality images of the nanocomposites.

Prior to imaging, very thin slices of the impregnated resin are taken. This is done using an ultra-microtome with a cryo-cutting attachment (Leica UC7 ultramicrotome with the FC7 chamber for cryo-ultramicrotomy). The newly added cryo-cutting attachment allows for much thinner slices to be taken (30-50 nm). Prior to cold-cutting, the soft resin material was unable to be sliced thinner than 100 nm, which made TEM imaging difficult. The ultra-thin slices are placed on TEM copper grids and carbon coated to reduce movement during imaging. The high-power electron beam can cause the resin slices to drift and shake, making imaging more difficult.

CHAPTER III

NANOPARTICLE CHARACTERIZATION

CdSe Quantum Dots

Figure 5 shows the absorbance and photoluminescence spectra of the dots as well as a TEM showing the fringing. The distinct exciton peaks at 560 nm and 590 nm in the absorbance plot indicate that the synthesis yielded a monodisperse sample. This is further backed up by a narrow (~50 nm) photoluminescent peak, a broad peak would be characteristic of a large variation in the diameter of the QDs. The TEM image of QDs that were drop cast on the copper substrate show uniform size and lattice fringing. The lattice fringing provides insight into the crystal structure of the QDs, another method of verifying that the synthesis was successful. XRD analysis shows peaks corresponding to that of hexagonal CdSe, indicating that a wurtzite crystal structure is present.

By using the location of the exciton peaks, one can determine the diameter of the QDs, as the absorption and emission are tunable by the size of the particle. In this case, the synthesized dots are 3.5 nm in diameter on average.

The top inset shows a single CdSe quantum dot, the lattice spacing is determined to be 3.5 Å using ImageJ software. The lower inset in figure 5b shows the QD stock solution under UV illumination. The solution has a low PLQY (<10%) due to surface losses and other loss pathways. In order to increase the quantum yield, a shell must be grown around the CdSe core.

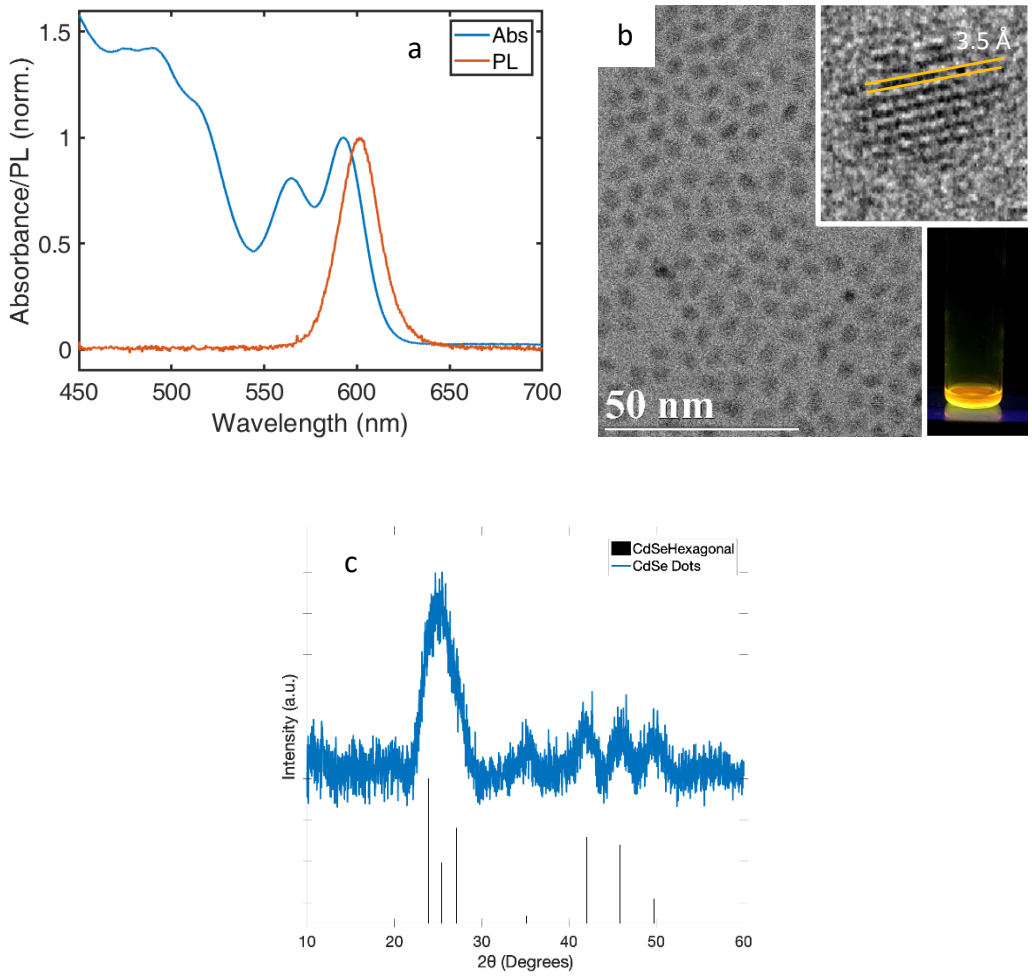

Figure 5: a) Plot of absorbance and photoluminescence spectra of CdSe quantum dots. b) TEM of CdSe quantum dots, inset shows lattice fringing of CdSe QDs. c) XRD data compared to a CdSe hexagonal reference.

CdSe/CdS Dot-In-Rod Heterostructures

Figure 6 shows the UV-vis absorbance and photoluminescence spectra as well as a TEM image of the dot-in-rod heterostructures. Features corresponding to shell and core absorption were observed at 450 nm and 600 nm respectively. The narrow PL peak at 610 nm is indicative of CdSe core emission. Shelling of the CdSe seeds was found to increase the PLQY up to ~70%. The dimensions of the NRs were calculated to be 44 nm x 4 nm, corresponding to an aspect ratio

of 11. The upper inset in figure 6b shows fringing in the CdS shell. XRD analysis confirmed the wurtzite crystal structure of the CdS shell with a lattice spacing of 3.5 Å.

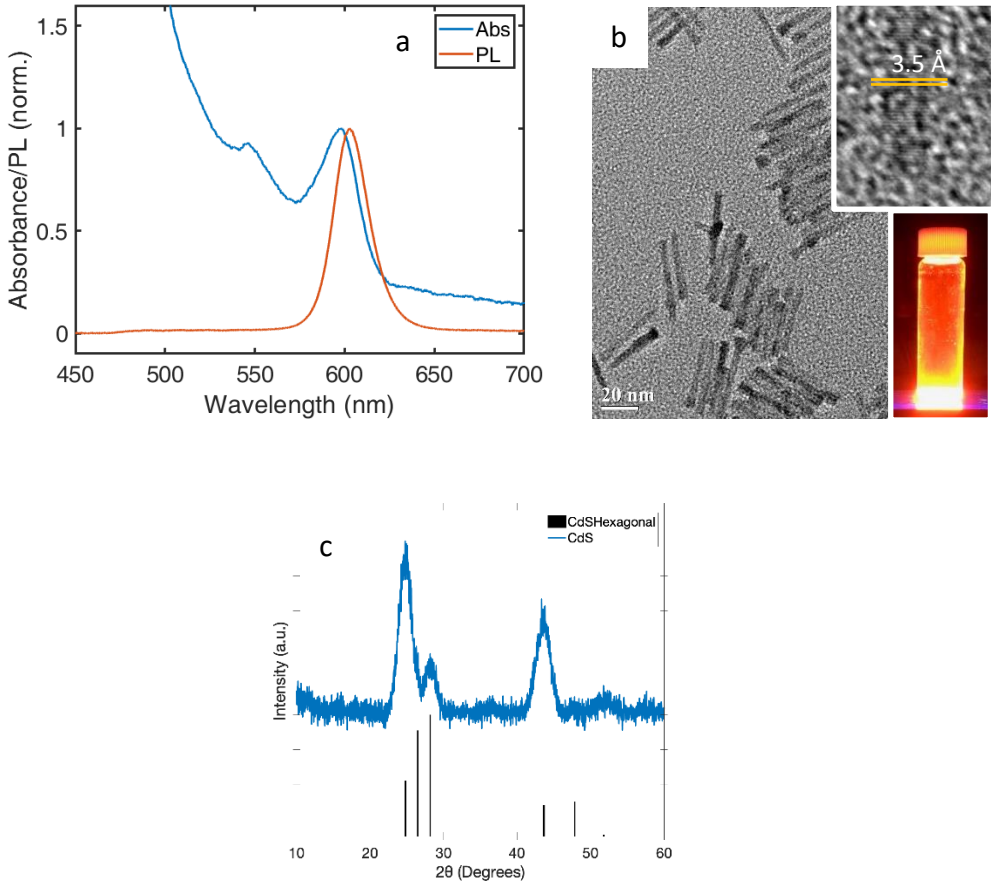

Figure 6:a) Plot of absorbance and photoluminescence spectra of CdSe/CdS dot-in-rod nanorods. b) TEM of CdSe/CdS dot-in-rods. (inset) image showing high photoluminescent quantum yield of CdSe/CdS sample. c) XRD data compared to a CdSe hexagonal reference

CHAPTER IV

OPTICAL QUALITY UV-CURABLE RESINS

Material Selection

UV-curable polymers have become a popular choice for nanocomposite production in recent years. A photopolymer is generally composed of three components, a monomer or polymer, an oligomer or cross-linking agent, and a photo-initiator. Upon exposure to high energy photons, the photo-initiator compounds decompose into radicals that supply the energy needed to convert the monomers/polymers and cross-linking agents into a complete polymer network. IRGACURE 819 (Diphenyl(2,4,6-trimethylbenzoyl)phosphine oxide) is the photo-initiator selected for this resin formulation. At a concentration of 0.1 wt%, it absorbs strongly at wavelengths below 440 nm and dissociates into radicals via cleavage forming up to four radical species that can initiate polymerization. A very small amount of initiator is needed, in this case 0.1 wt%, and no terminating agent is needed to stop the reaction.

A UV-curable resin or photopolymer was selected as the polymer matrix for this nanocomposite due to its relatively small volume change and facile curing conditions. A UV-curable resin was also selected because it allows the curing to be done at ambient temperatures in the presence of air and the polymerization rate can be controlled using the intensity of light. Solvent based polymers and thermosets were considered for this study, but their curing conditions would have made film production difficult while applying an electric field. Solvent evaporation that occurs during the hardening of solvent based polymers would be slow due to the design of the sample cell. Similar works have found success with these polymers by replacing the top ITO slide with a porous top contact such as a Teflon coated stainless steel mesh.[18]

The resin is composed of the monomer lauryl methacrylate (LMA) and cross-linking agent ethylene glycol dimethacrylate (EGDM), as well as a photo initiator (IRGA 819). By varying the ratios of LMA to EGDM, properties of the film can be controlled. The higher the concentration of cross-linking agent in the mixture, the tighter and more interconnected the matrix is after curing.

Formulation & Thickness Optimization

During this study, the wt% ratios of LMA to EGDM were swept from 3:1 to 10:1. The soft films produced by the 10:1 wt% ratio made sample characterization difficult, likely due to a lack of cross-linking agent. The films produced with a 3:1 ratio presented the opposite properties; they were too brittle for handling and characterization as the polymer network was very tightly bound. It was determined that the ratio of 5:1 resulted in a thin film that was hard enough to be sliced thinly, while being soft enough to avoid excessive cracking during handling. Although mechanical testing was not done to provide solid justification, it can be said that the films become increasingly brittle and stiff as the wt% of the cross-linking agent is increased. On the microscopic level, as more cross-linking occurs between PLMA (poly-LMA) chains the resulting network becomes denser and more interconnected, allowing for much less movement between polymer chains. This hypothesis is in agreement with the observed film characteristics. The mechanical properties of the films were not examined during this study.

All mixing must be done under inert atmosphere to avoid photobleaching during curing. Image 7 shows the effects of air in the resin during curing, each of the solids produced in the image are of the same resin formulation. The non-fluorescent solids shown in the figure were mixed completely outside of the glovebox while the brightest were mixed under an inert

atmosphere in the glovebox. The combination of oxygen and UV light during cured results in oxidation and degradation of the nanorods. The photoluminescence is quenched due to the degradation and results in the non-fluorescent samples.

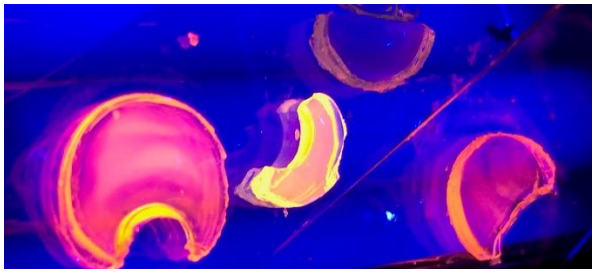

Figure 7: Cured nanocomposites showing the effect of curing conditions on sample fluorescence.

Lamp intensity is an important factor when curing photopolymers. Photo-DSC studies have shown that heat flow and respective reaction rates increase as UV light intensity increases.[19] The spot curing lamp used in this study is capable of intensities as high as 18 W/cm^2 at the tip of the light guide. Figure 8 shows the lamp intensity and spot size as a function of distance from the waveguide tip. While this extreme intensity would lead to a high rate of reaction, the temperatures that accompany the high intensity light instantly cause the sample cell to crack and break. To maintain the integrity of the cell, much lower intensities (~100 mW/cm^2) are used when curing resin sample. This is not ideal, as the lower power diminishes the rate of reaction and makes it less likely that the timescale of curing (seconds) matches that of the alignment of the NRs (milliseconds).

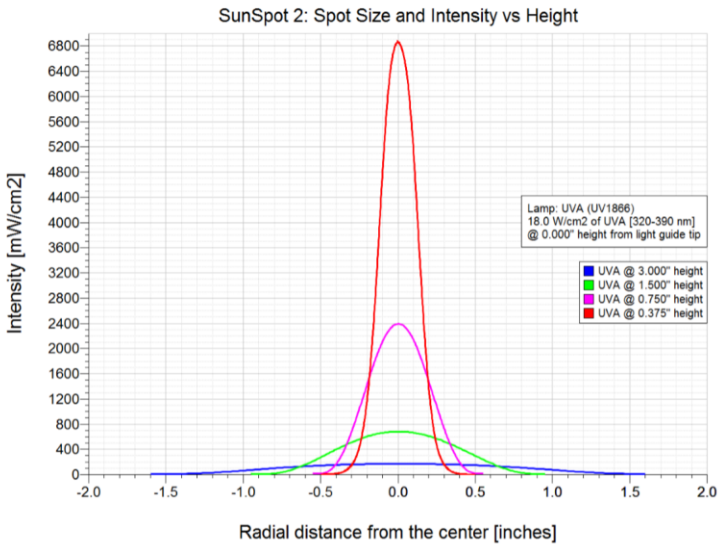

Figure 8: Sunspot 2 UV lamp intensity and spot size at given distances from the wave guide tip.

Film thickness is the most important parameter for the resin thin films produced in this study. As film thickness decreases, the higher the likelihood of achieving quantifiable alignment of NRs in the resin films. Recent progress has allowed for the production of thin films with a thickness of 50 µm. The success is being attributed to sonicating the resin mixture just prior to injecting it into the sample cell for curing. The sonication causes intense vibrations in the molecules and ensures that complete mixing is achieved. Prior to this new sample treatment, viable films could not be produced thinner than 100 µm.

CHAPTER V

FULL ALIGNMENT OF NANORODS

Alignment in Dodecane

Prior to studying alignment of the NRs in resin, alignment was first explored in dodecane. A colloidal dispersion of NRs in dodecane was loaded into a sample cell with 50 μm spacer beads. It is important to know that the crystal growth during the hot injection synthesis results in some NRs having a permanent charge. Due to this, AC fields should be used instead of DC fields to avoid aggregation at the ITO electrodes. Another action that must be taken to avoid aggregation at the electrodes is to work with field frequencies higher than the transit time of the NRs. The transit time is a function of the spacing between ITO panels and the applied electric field, for this case it has a value of approximately 5 ms.[20] A sinusoidal function with a frequency of 2 kHz was selected for the full alignment study in dodecane.

In this study, the relative absorbance was calculated as a function of field intensity. Starting at no field, the strength was incrementally increased until a short circuit occurred and destroyed the cell. The best case during this series of trials resulted in a max strength of approx. 30 V/μm. The relative change in absorbance showed a major decreasing trend as the field strength increased. By understanding the relationship between the electric field and the average orientation of the NRs, one can see why the absorption decreased with increasing field strength. As the NRs become aligned in solution parallel to the electric field, their long axis becomes perpendicular to the electric field of the incident light. The higher depolarization factor of the short axis results in less light absorption.[20] The rate at which the relative absorption decreases begins to plateau as the field strength approaches 10 V/μm and eventually reaches zero at

approximately 15 V/µm. This leads us to believe that full alignment has been reached for the CdSe/CdS-dodecane system. Full alignment is defined as the point where the relative change in absorbance no longer changes as the field strength increases, at this point alignment is said to be saturated.

Figure 9 displays the relative change in absorbance as a function of electric field strength. The slope of the line approaches zero at approximately 15 V/µm, showing that the relative absorbance is at a minimum and no longer controlled by the applied field strength. Literature reports full alignment being reached at 17 V/µm for a similar system using CdSe/CdS NPs with a smaller aspect ratio.[20] The values are not expected to match exactly, as different aspect ratios and solvents are used. The effect of the aspect ratio on degree of alignment was not studied during this experiment.

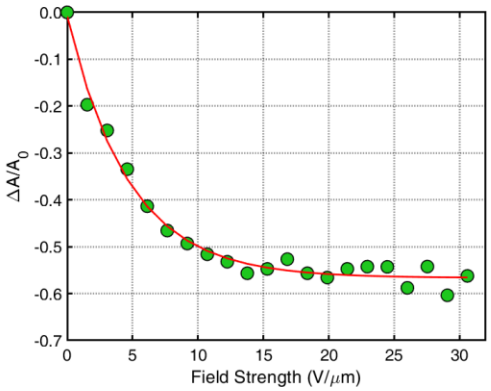

Figure 9: Complete alignment study in dodecane showing relative absorbance as a function of field strength.

Figure 10 shows the time-dependent relative absorbance due to an applied field signal corresponding to the point 24.48 V/µm on the previous figure. The red line shows the applied sinusoidal function. As the field strength becomes nonzero, the relative absorbance quickly drops

until it reaches a trough. The troughs represent the portion where the rods are fully aligned while under the influence of the field (24.48 V/µm at max). If a line is extrapolated from the onset of the trough down to the field strength plot, the intersection point is where the field strength is approx. 15 V/µm. This is also true for the point when the trough ceases to exist, and relative absorbance begins to be less negative. A similar trend is seen in literature under comparable electric field strength and frequency.[20]

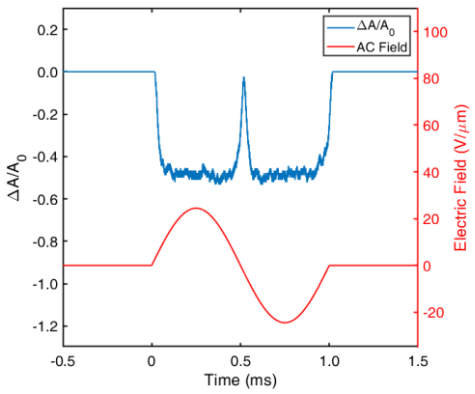

Figure 10: Sample response to a single wave pattern as an indication of full alignment. The red plot shows the applied electric field. The blue plot shows the relative absorbance response signal.

The two images shown in figure 11 and provide a valuable visual insight into the angular distribution of fluorescence emission from a sample under field alignment. Image 11a shows a solution of NRs in a sample cell under UV illumination with no field applied (E = 0). The fluorescence emission of the sample appears to be isotropic. This confirms the random orientation of NRs in the sample. Image 11b shows the same sample under an AC electric field of approximately 24.48 V/µm. In this case, the angular distribution of fluorescence emission exhibits an anisotropic pattern: the fluorescence intensity normal to the cell surface is significantly decreased. This anisotropic emission profile is strong evidence for the NRs being in

a state of complete alignment when exposed to a strong electric field, as they emit preferentially from their long axis. The ITO sample window in figure 11b appears to have very limited fluorescence emission normal to the surface, any fluorescence is likely due to some aggregation at the surface. This is interesting due to the fact the while the field is being applied there are times when the field is equal to zero, yet the emission does not look like that of figure 11a. It is hypothesized that the time spent unaligned is small compared to the time spent aligned, resulting in an average emission profile dominated by the aligned emission conditions.

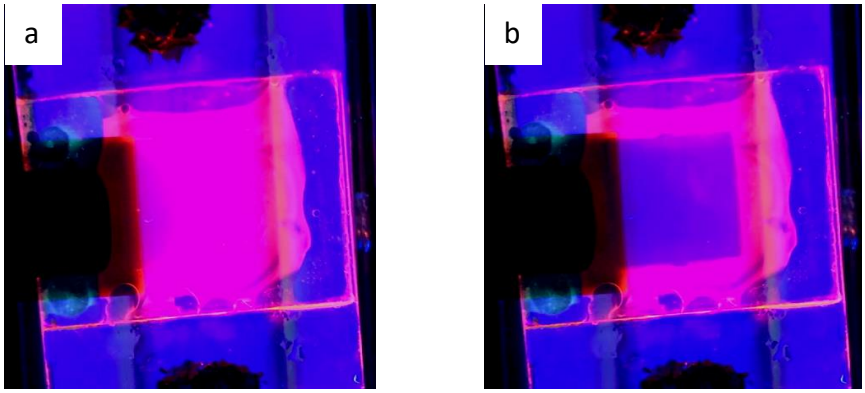

Figure 11: ITO sample cell with CdSe/CdS NRs in solution. a) sample with no applied electric field. b) sample cell with an applied electric field of approx. 25 V/µm

Figure 12 has been added as a tool to visualize the orientation of the rods in the sample cell under both conditions. With no field applied, the rods are randomly oriented and controlled by Brownian motion, relating to figure 11a. Under the presence of the electric field, the rods are held so that their long axis are parallel to the electric field.

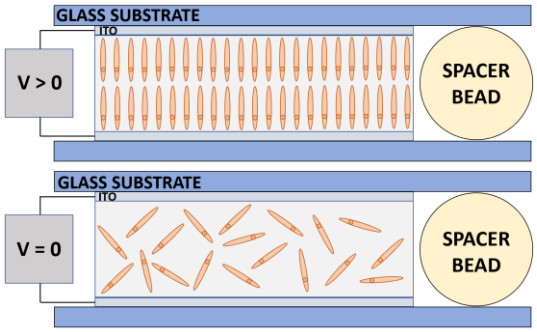

Figure 12: Schematic showing the rod orientation in the presences of a strong electric field (top) and under no field conditions (bottom)

Alignment in Resin

The alignment study was repeated using the 5:1 LMA to EGDM resin with no IRGA 819 instead of dodecane. By not incorporating 0.10 wt% of the photo-initiator, the same 405 nm laser can be used without the sample polymerizing during the measurement. The resin had 0.05 wt% NRs incorporated using sonication and a 50 µm sample cell was used. Figure 13 shows the applied sinusoidal AC electric field and the response signal indicating the respective change in relative absorbance. As shown in the previous study, the change in relative absorbance approaches zero as the field strength passes through zero. Unlike the alignment study in dodecane, full alignment was not reached and there is not a visible trough like the one seen in figure 10. The study was encouraging, in that the relative absorbance does decrease as the field strength increases. Figure 14 shows the trend of decreasing relative absorption up to the value of approximately -0.3, where it begins to level out and then increase. This behavior is not expected and is likely due to an error with the function generator or the high voltage amplifier. As the function generator output increases past 3 V (field strength of 9.2 V/µm) the oscilloscope readout

shows a phase inversion and the response signal stops following the expected trend. This continues to happen until the cell is destroyed due to electrical shorting. Further testing of the alignment in resin will be completed after phase inversion problem is addressed.

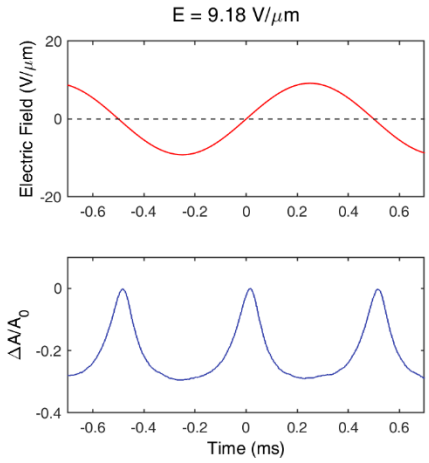

Figure 13: The sinusoidal input voltage and corresponding relative absorbance value of the NRs in resin (Max field strength = 9.18 V/µm).

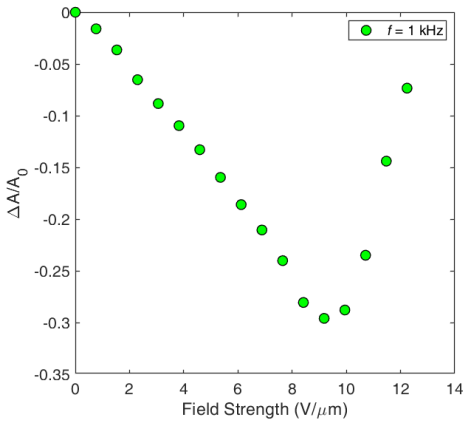

Figure 14: Relative absorbance as a function of field strength of NRs dispersed in LMA/EGDM without IRGA 819

Visual evidence of alignment is seen when placing the sample cell over the UV stage as done in the previous alignment study. Figure 15 shows the two states where a) is the sample cell with no electric field being applied and b) shows the fluorescence profile with an applied voltage

of approx. 10 V/µm. While the fluorescence is decreased out of the normal face of the sample cell, it is not completely diminished like that of the dodecane study. This is further evidence that complete alignment has not been reached for this study. However, this does indicate that alignment is possible in the selected resin medium.

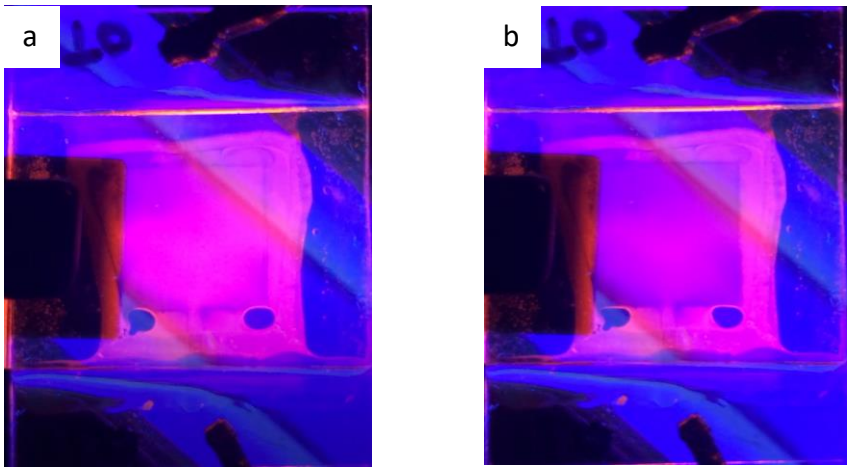

Figure 15: Resin sample cell showing a) the fluorescence profile with no field applied and b) the fluorescence profile with a field of approx. 10 V/um

CHAPTER VI

NANOCOMPOSITE PRODUCTION

Incorporating Nanorods Into Resin

The LMA/EGDM UV-curable resin material produces optically clear thin films using the weight % ratio of 5:1 LMA to EGDM. Figure 16 shows the clarity of the films with and without NRs solubilized in the material. Prior to the addition of NRs, the films have a light-yellow color. The addition of the NRs creates a more intense yellow/orange color that becomes more visible as the concentration of the NRs is increased. Literature states that for this photopolymer compound, a wt% of 0.05 is the optimum CdSe/CdSe NRs concentration in the matrix.[21] The concentration of the stock solution is unknown due to a spill that occured during cleaning. A solution to this problem was to add small amounts of the stock solution to a vial and evaporate the hexane solvent, leaving just the NRs behind. By weighing the vial on a high precision balance after each small addition, it was determined approximately 1.550 mL of stock solution results in 0.250 mg of NRs, or 0.05 wt% when using 1.000 g of LMA. This NR concentration was held constant throughout the entire alignment/nanocomposite study.

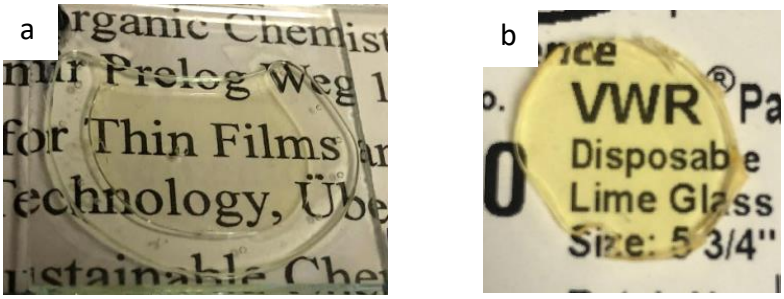

Figure 16: Images showing the optical clarity of the resin thin films doped films a) without NRs and b) with embedded NRs.

Although the concentration is constant in each film, the relative concentration was not constant across the entire individual film. Concentration gradients formed in the samples while curing the resin under an applied electric field. This gradient can be seen in figure 17 when the cured sample (1 mm thick) is placed on a black light stage. A hypothesis is that the gradient is an artifact of the electric field because it is not present in the control samples cured under zero field conditions. A proposed explanation for this concentration gradient is that the rods are forming agglomerates due to the electric field presence during curing, rather than forming a monodispersed nanocomposite. The formation of aggregates under an applied field is seen in literature. A study by Pietra et al. examining the behavior of CdSe/CdS core/shell NRs under applied magnetic fields, showed that formation of aggregates amplifies the effect of the applied field making it easier to become aligned.[22] This was only seen in NRs with high aspect ratios (comparable to ours) due to the stronger side to side interactions. If aggregates are forming from the application of magnetic fields, it is likely that a similar process is occurring with the application of an electric field. The formation of concentration gradients or potential aggregates has been seen in multiple instances, both visually and while imaging the samples using TEM. The TEM images and will be discussed further in the next chapter.

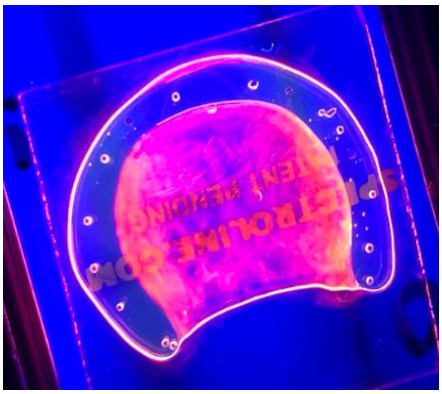

Figure 17: Resin nanocomposite over a black light to show the presence of concentration gradients.

The concentration gradient seems to become less prevalent, or at least less visible, as the film thickness is decreased. However, a new problem is encountered when working with the thinner films (<200 µm). During curing, small rifts form in the film where it appears the sample has pulled away from the ITO sample cell. Films with these rifts cannot be removed from the sample cell for characterization. This behavior can be seen in figure 18, which shows a sample cell after curing under a field of approximately 10 V/µm. This is thought to be caused by a small reduction in volume during the resin curing process due to this being observed in resin samples cured under no-field and field conditions. However, the presence of an electric field exacerbates the problem as it occurs in most of the samples cured with an applied field.

The volume reduction during photopolymerization has been studied by Tomita et al. who found that polymer shrinkage of up to 10% can occur during curing. This was measured using a novel spectral interferometric method. The shrinkage is a product of the reduction of free volume between monomers as they are polymerized, where the van der Waals spacing between monomers is replaced by covalent bonding in the polymer network.[23]

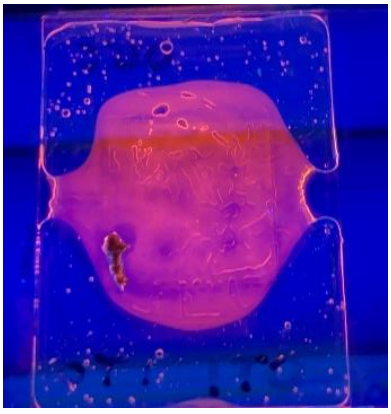

Figure 18: Resin nanocomposite cured under electric field showing signs of non-uniform surface voids.

Sonication of the resin and NR mixtures for 30 minutes prior to loading into the sample cell has greatly reduced the effects of shrinkage and concentration gradients present in the films. Figure 19 shows the highly fluorescent nature of the nanocomposite thin films (200 μm) produced after sonicating the resin and curing without the presence of an electric field (E=0). The effects of sonication will be highlighted in the follow TEM analysis chapter.

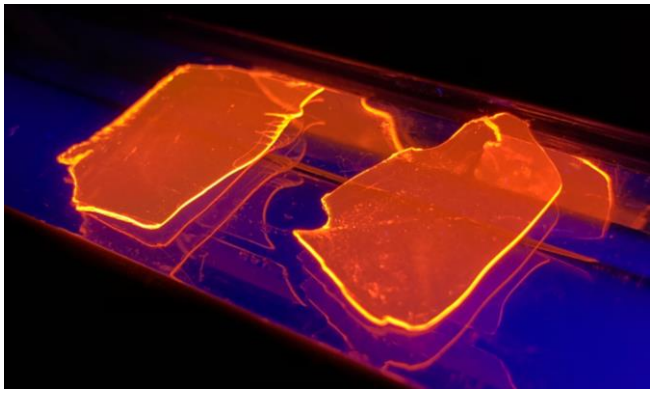

Figure 19: Control thin films (200 um) with NRs dispersed via sonication for 30 minutes, imaged over a black light.

Ordered Nanocomposite Production

After optimizing the production of nanocomposite thin films, the next step is to cure the films while applying an electric field to induce a degree of order in the NRs. This film production setup is similar to the analysis of NR alignment in the resin mixture, expect in this study the photo-initiator is present and the film is not probed using a laser. Instead, the sample cell is placed under UV-curing lamp and attached to the high-voltage electrodes.

An important aspect of producing ordered nanocomposites is selecting the best waveform to induce alignment while curing. In this study we have cured resin samples with a variety of waveforms ranging from an AC sinusoidal signal to a pulsed DC square-wave. Literature has provided evidence that the CdSe/CdS NRs possess a permanent dipole. Mohammadimasoudi et al. explained that if the only torque generated by the electric field was from the dielectric of the material, a field strength of 40 V/μm, instead of 17 V/μm they report, would be needed to induce complete alignment of CdSe/CdS heterostructures of almost the same dimensions.[20] Another study done by Liang-shi Li showed that the transient electrical birefringence curve of CdSe NRs have asymmetric falling and rising edges which indicate the presence of a permanent electric dipole moment along the long axis of the particle.[24] Working under the assumption that the NRs have a permanent dipole, it seems that a pulsed DC would be the best waveform selection. As an AC field would cause the NRs to switch direction every half cycle of the waveform. It is noted that some particles will have a non-zero net charge and will migrate to their desired electrode, this is an unavoidable side-effect of the hot injection synthesis. To combat aggregation, a frequency is selected that is higher than the transit time of the NRs (5 ms or 200 Hz). Most curing is done with frequencies greater than or equal to 1 kHz.

Another important factor regarding ordered nanocomposite production is the thickness of the film. Thinner films allow for higher electric fields to be present during curing. The first potentially promising result was seen when comparing the fluorescence out of the normal face of the resins of a control and "aligned" 1000 μm samples. Figure 20 shows a comparison of the control sample and the sample cured under an electric field. Due to the thickness of this sample, the maximum field intensity possible is only 1.5 V/μm. Looking at the data from the alignment study in resin, this would only lead to a relative absorption value of -0.065, nowhere near the

value that is expected for complete alignment, -0.55. It is likely that the reduced surface emission is due to aggregation and concentration gradients present in the sample. This sample was produced prior to the implementation of sonication prior to curing. TEM analysis of the sample provides more evidence that aggregation was present in the sample, this will be discussed in the following chapter.

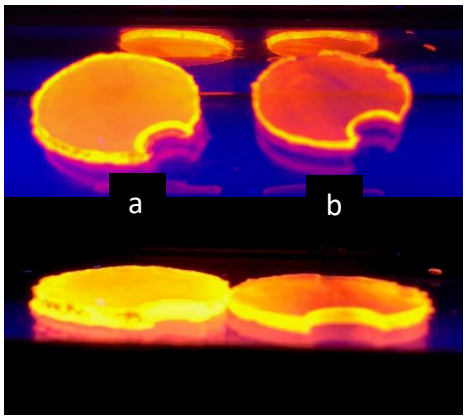

Figure 20: Side by side comparison of a) control sample and b) sample cured under an electric field (1.5 V/µm).

The most recent attempt to produce an ordered nanocomposite has early indications that some degree of alignment is present in the sample. This film is 50 µm thick and was cured under a field strength of approximately 10 V/µm using a pulsed DC current with a frequency of 1 kHz. The duty cycle was set to 80/20, meaning the field is applied for 0.8 ms and then turns off for 0.2 ms before being applied again. The applied field is either positive or zero, so no switching of the NRs occurs due to their permanent dipole. Figure 21 shows a comparison between a) the control film made from the same batch of resin and of the same thickness (50 µm) and b) the film cured under an electric field (12.24 V/µm). Looking at the alignment in resin study, a field of that

strength corresponds to a relative absorption value of -0.3. This value is much closer to that of full alignment (approx. -0.55).

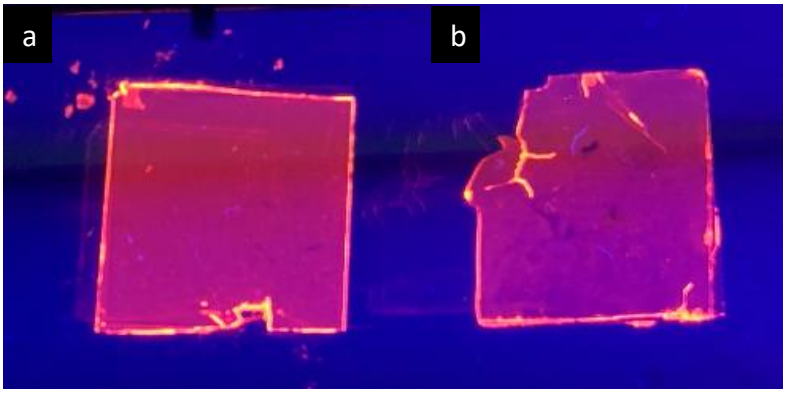

Figure 21: Comparison of a) control 50 um film cured under no field and b) 50 um film cured with a field strength of 12.24 V/um.

Another promising aspect of this study is that the film was cured under the same field strength that produced a visible change in fluorescence normal to the sample surface, as shown in the images in the "alignment in resin" section. To test if the aligned film has more transmission through the normal face than that of the film than the control film, a simple experiment was designed. A laser was shone through three different films with a thickness of 50 µm; the control and aligned films shown in figure 21 and a neat resin film (5:1 LMA/EGDM) with no NRs. The strength of the laser was measured using the photoreceiver from the optical setup and the response voltage was recorded. Figure 22 shows a plot of the transmittance for the control and aligned films, using the neat film as a blank. The control film and aligned film have mean transmittances of 95.9% and 97.3% respectively. A lower transmittance is expected for a film with particles aligned normal to the surface, indicating that the "aligned" film may have some degree of alignment. While this test is not conclusive, it does prove that there is the possibility of

aligned particles being present in the sample. The final step in this study is to look at slices of this film using TEM to gain an understanding of the actual orientation of the NRs in this nanocomposite.

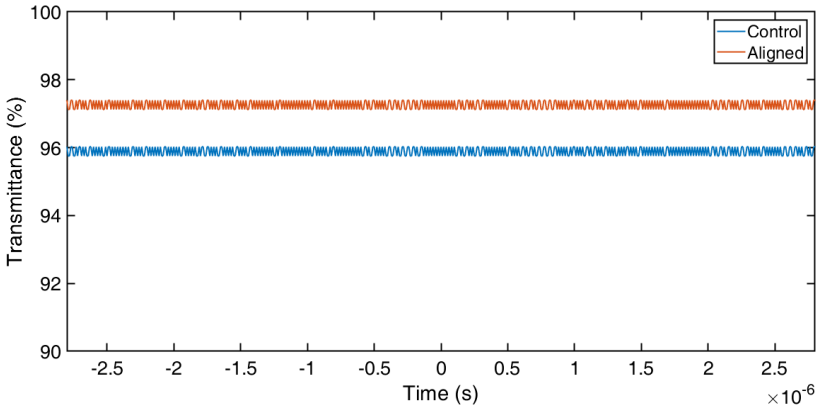

Figure 22: Transmittance plots for the control and aligned 50 um films of 5:1 LMA:EGDM

CHAPTER VII

CHARACTERIZATION OF NANOCOMPOSITES

TEM Imaging of Nanocomposite Films

The first is to directly image slices of the resin using TEM. By analyzing the images, one can generate an order parameter based on the orientation of a collection of rods relative to the direction of the applied electric field. For the order parameter to be determined, two data points must be taken from the TEM images. As shown in the example in figure 22, the electric field direction must be established along with the average rod orientation. The angle between these two vectors is used in the calculation of the order parameter, with S =1 being indicative of complete alignment.

$$S = 1 - \cos^2 \theta_{avg} \quad (2)$$

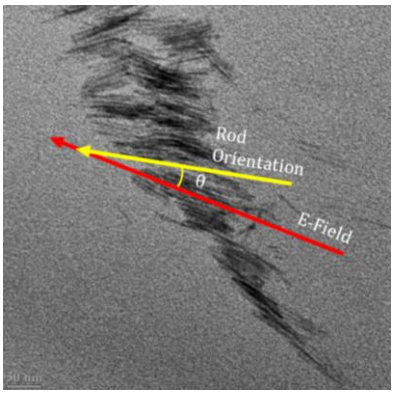

Figure 23: Sample TEM showing how the order parameter would be calculated using the electric field direction, average rod orientation and the angle between the two.

The thin resin slices were produced using a cryo-ultramicrotome. This instrument utilizes a diamond knife to take slices of resin with thicknesses ranging from 30-250 nm. Ideally, taking the thinnest slices of resin possible allows from the best TEM images to be produced. The increased thickness leads to scattering of the electron beam and results in lower image resolution. In addition to using thin slices, the samples are carbon coated after being loaded on the TEM grid. This reduces movement of the samples caused by the higher energy electron beam.

Early studies completed before the addition of the cryo-cutting attachment to the ultramicrotome yielded low resolution images of the rods in solution. Without the low temperature induced stiffness of the material, the resin was too soft for thin slices (30-50 nm) to be taken. The image in figure 23 shows the low resolution TEM taken of a 150 nm thick slice. The image shows a large aggregate of NRs all preferentially aligned along their long axis due to interparticle forces. While the aggregates may be easier to align in an electric field, this is not a desired characteristic of LSC materials.[22]

The thick polymer matrix, with its carbon backbones, has many scattering sites for the electron beam and makes it difficult to focus the beam on the NRs. As the path length of the electron beam through the resin is decreased, it is shown how the resolution is greatly improved.

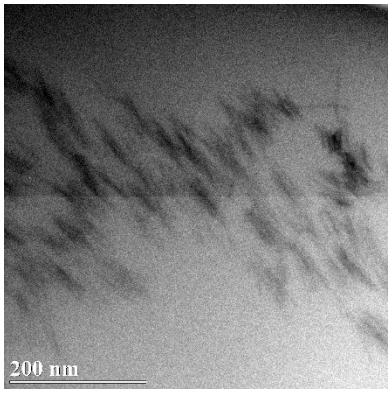

Figure 24: TEM of sample in figure 20b cured under a field of 1.5 V/um

With the addition of the cryo-attachment, much thinner slices of resin (<100 nm) could be taken and analyzed via TEM with minimal scattering. Figure 24 shows a high-resolution image of the NRs embedded in the resin matrix. The NRs are still aggregated side to side, as this issue had not been addressed at the time this image was taken. This resin sample had not been cured under an electric field which led us to believe that the aggregation was an artifact of improper mixing procedures.

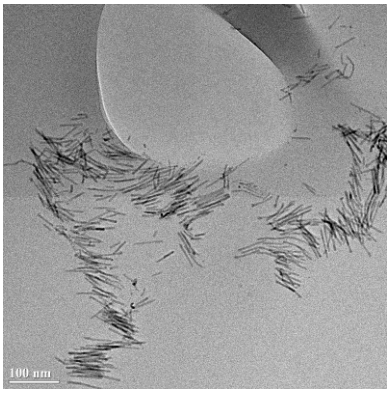

Figure 25: TEM of a slice of resin control film (E = 0) that is <100 nm thick, shows increased resolution.

Aggregation of nanoparticles in polymer resins is a common issue in nanocomposite production. Throughout literature, a common fix to reduce aggregation is to sonicate the mixture instead of mixing. Sonication utilizes high frequency sound waves to induce mixing in solution by causing the NPs to vibrate and increases intermolecular spacing. In our work, the resin mixtures are sonicated for 5-30 mins in a sonication bath. Longer sonication times are avoided, as degradation of the particles could occur. Figure 25a shows a TEM image of a 30 nm slice of the 200 µm control film shown in figure 19. This is clear evidence that sonication greatly reduces

aggregation of the NRs in resin, of the 25+ TEM images taken of this film there was no aggregation present. Figure 25b shows an additional finding, sonication prior to the application of an electric field inhibits aggregation from occurring due to an applied electric field.

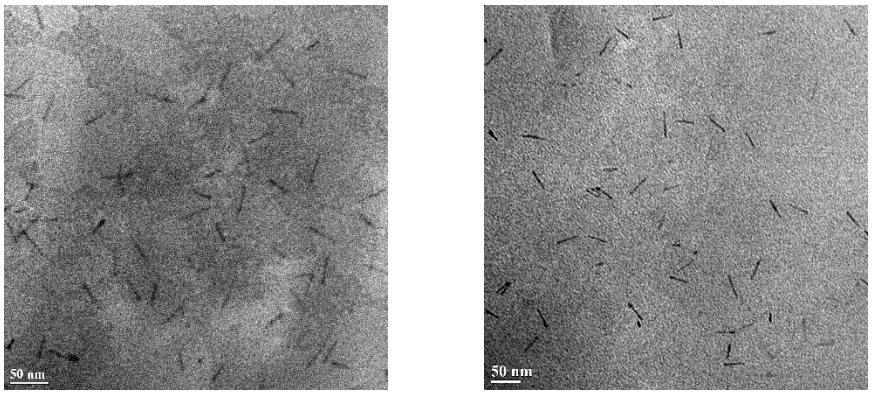

Figure 26: TEM image of 30 nm thin slice of a) 200 um control film (E=0) and b) cured under a field of 7.65 V/um showing no aggregation after sonication for 30 mins.

The deviation of NRs with respect to the direction of the applied electric field (θ_{dev}) was calculated by analyzing TEM images of an aligned 200 μm film. Rods from nine different locations of a thin film slice were analyzed. The histogram (Figure 26) represents the distribution of deviation angles of 264 rods. This analysis yielded no clear trend and indicates that alignment is not present in this sample.

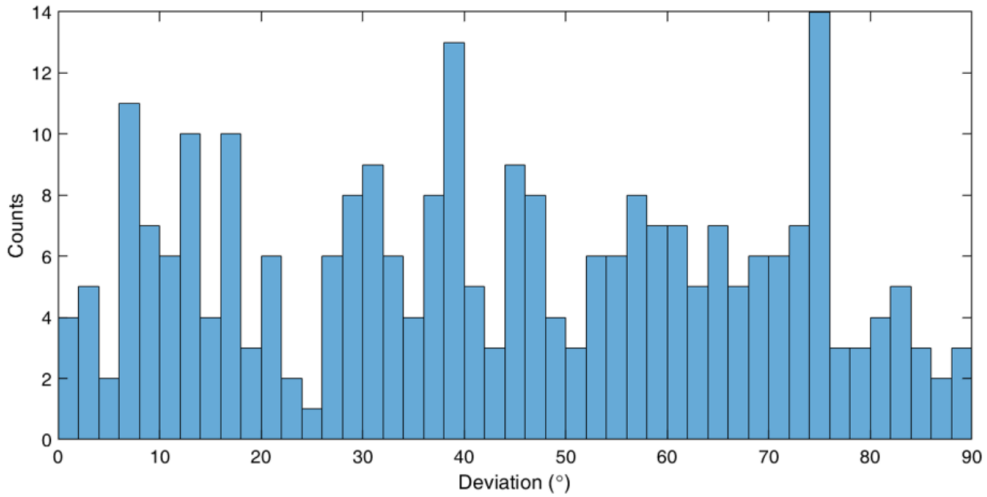

Figure 27: Histogram of deviation from E-field direction for 264 rods imaged using TEM.

Modeling Fluorescence Anisotropy

Fluorescence anisotropy offers an alternate method for determining the degree of alignment in solid samples. The theoretical value of anisotropy for a completely random distribution of dipole-emitters has been derived to be 0.4.[25] However, the corresponding value for an "aligned" sample would depend on the mean orientation of NRs and the degree of alignment. Assuming ideal dipole behavior and a fixed mean orientation, the anisotropy of a CdSe/CdS NR ensemble was calculated as a function of order parameter (Figure 27). The alignment of NRs was modeled using a Von Mises-Fisher distribution where the order parameter (κ) controls the degree of alignment. This model can be applied to experimental data in order to approximate the degree of order in aligned nanocomposites.

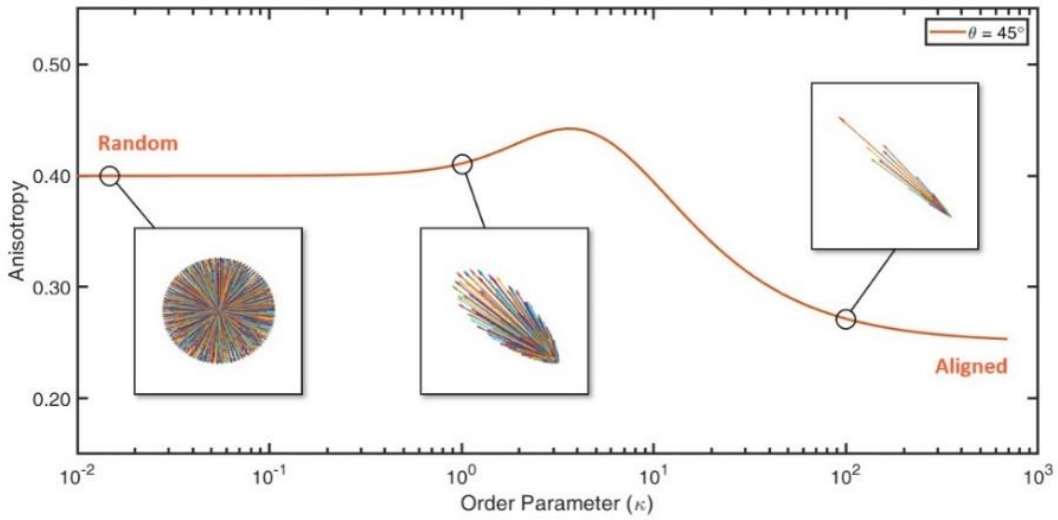

Figure 28: Computational model showing order parameter as a function of anisotropy and film orientation.

As is evident from the above figure, the correlation between anisotropy and order parameter does not always guarantee a one-to-one mapping. However, by varying the orientation of alignment through a range of polar angles (θ), a unique trend can be generated for any given value of order parameter.

CHAPTER VIII

CONCLUSIONS

In this thesis, the application of aligned anisotropic nanoparticles for solar concentration was investigated. The goal of this research was to align CdS/CdSe dot-in-rod nanoparticles using an electric field and to immobilize them in a UV-curable resin thin film.

CdSe QDs and CdSe/CdS dot-in-rod heterostructures were successfully synthesized via hot injection techniques and fully characterized using UV-vis, TEM and XRD. The NRs were aligned in solution and in resin using an externally applied electric field. Orientation of the NRs was probed by measuring the concurrent change in absorption in response to an applied election field. Complete alignment was achieved in solution as shown by the saturation of the change in relative absorption as a function of electric field, with full alignment present in fields higher than 15 V/μm. Complete alignment was not achieved for the NRs in resin.

Optical clarity thin films, as thin as 50 μm, were produced using a UV-curable resin composed of a 5:1 wt% ratio of LMA:EGDM with an IRGA 819 photo-initiator. Highly fluorescent nanocomposites were produced by incorporating the NRs into the resin compounds. Monodispersed samples were achieved by sonicating the resin compounds before synthesis. UV-curable resin thin films embedded with NRs were cured in the presence of an electric field to produce potentially ordered nanocomposites. The orientation of the NRs in resin were probed using TEM imaging of slices of resin taken by an ultra-microtome. Currently, alignment has not been confirmed in the cured films.

Future works include taking TEM images of the 50 μm resin film that has shown promising evidence of alignment. The TEM data will allow the calculation of an order

parameter. An experiment is proposed that probes the film's fluorescence anisotropy and compares against a computational model to determine an order parameter.

REFERENCES

1. Schneider, K., New World Record for Solar Cell Efficiency at 46%. Fraunhofer Institute for Solar Energy Systems ISE.; 2014.

2. Debije, M.; Verbunt, P. P. C., Thirty Years of Luminescent Solar Concentrator Research: Solar Energy for the Built Environment. *Advanced Energy Materials* **2012,** *2* (1), 12-35.

3. MacQueen, R. W.; Cheng, Y. Y.; Clady, R. G. C. R.; Schmidt, T. W., Towards an aligned luminophore solar concentrator. *Opt. Express* **2010,** *18* (S2), A161-A166.

4. Verbunt, P. P. C., *Light management in luminescent solar concentrators :aligned organic dyes and organic wavelength selective reflectors*. 2012. Eindhoven: Technische Universiteit Eindhoven DOI: 10.6100/IR740226

5. Verbunt, P. P. C.; Kaiser, A.; Hermans, K.; Bastiaansen, C. W. M.; Broer, D.; Debije, M., Controlling Light Emission in Luminescent Solar Concentrators Through Use of Dye Molecules Aligned in a Planar Manner by Liquid Crystals. *Advanced Functional Materials* **2009,** *19* (17), 2714-2719.

6. Hens, Z.; Moreels, I., Light absorption by colloidal semiconductor quantum dots. *Journal of Materials Chemistry* **2012,** *22* (21), 10406-10415.

7. Yong, K. T.; Sahoo, Y.; Swihart, M. T.; Prasad, P. N., Growth of CdSe Quantum Rods and Multipods Seeded by Noble-Metal Nanoparticles. *Advanced Materials* **2006,** *18* (15), 1978-1982.

8. Krahne, R.; Morello, G.; Figuerola, A.; George, C.; Deka, S.; Manna, L., Physical properties of elongated inorganic nanoparticles. *Physics Reports* **2011,** *501* (3), 75-221.

9. Talapin, D. V.; Koeppe, R.; Götzinger, S.; Kornowski, A.; Lupton, J. M.; Rogach, A. L.; Benson, O.; Feldmann, J.; Weller, H., Highly Emissive Colloidal CdSe/CdS Heterostructures of Mixed Dimensionality. *Nano Letters* **2003,** *3* (12), 1677-1681.

10. Talapin, D. V.; Shevchenko, E. V.; Murray, C. B.; Kornowski, A.; Förster, S.; Weller, H., CdSe and CdSe/CdS Nanorod Solids. *Journal of the American Chemical Society* **2004,** *126* (40), 12984-12988.

11. Ghezelbash, A.; Koo, B.; Korgel, B. A., Self-Assembled Stripe Patterns of CdS Nanorods. *Nano Letters* **2006,** *6* (8), 1832-1836.

12. Querner, C.; Fischbein, M.; Heiney, P.; Drndić, M., Millimeter-Scale Assembly of CdSe Nanorods into Smectic Superstructures by Solvent Drying Kinetics. *Advanced Materials* **2008,** *20* (12), 2308-2314.

13. Baker, J. L.; Widmer-Cooper, A.; Toney, M. F.; Geissler, P. L.; Alivisatos, A. P., Device-Scale Perpendicular Alignment of Colloidal Nanorods. *Nano Letters* **2010,** *10* (1), 195-201.

14. Zanella, M.; Gomes, R.; Povia, M.; Giannini, C.; Zhang, Y.; Riskin, A.; Van Bael, M.; Hens, Z.; Manna, L., Self-Assembled Multilayers of Vertically Aligned Semiconductor Nanorods on Device-Scale Areas. *Advanced Materials* **2011,** *23* (19), 2205-2209.

15. Singh, A.; Gunning, R. D.; Ahmed, S.; Barrett, C. A.; English, N. J.; Garate, J.-A.; Ryan, K. M., Controlled semiconductor nanorod assembly from solution: influence of concentration, charge and solvent nature. *Journal of Materials Chemistry* **2012,** *22* (4), 1562-1569.

16. Amit, Y.; Faust, A.; Lieberman, I.; Yedidya, L.; Banin, U., Front Cover: Semiconductor nanorod layers aligned through mechanical rubbing (Phys. Status Solidi A 2/2012). *physica status solidi (a)* **2012,** *209* (2).

17. Carbone, L.; Nobile, C.; De Giorgi, M.; Sala, F. D.; Morello, G.; Pompa, P.; Hytch, M.; Snoeck, E.; Fiore, A.; Franchini, I. R.; Nadasan, M.; Silvestre, A. F.; Chiodo, L.; Kudera, S.; Cingolani, R.; Krahne, R.; Manna, L., Synthesis and Micrometer-Scale Assembly of Colloidal CdSe/CdS Nanorods Prepared by a Seeded Growth Approach. *Nano Letters* **2007,** *7* (10), 2942-2950.

18. Guo, Y.; Batra, S.; Chen, Y.; Wang, E.; Cakmak, M., Roll to Roll Electric Field "Z" Alignment of Nanoparticles from Polymer Solutions for Manufacturing Multifunctional Capacitor Films. *ACS Applied Materials & Interfaces* **2016,** *8* (28), 18471-18480.

19. Dogruyol, S. K., Photo-DSC Investigation of Acetonaphthone Type Photoinitiators at Different Light Intensities. *Journal of Photopolymer Science and Technology* **2017,** *30* (6), 651-656.

20. Mohammadimasoudi, M.; Hens, Z.; Neyts, K., Full alignment of dispersed colloidal nanorods by alternating electric fields. *RSC Advances* **2016,** *6* (61), 55736-55744.

21. Bomm, J.; Buchtemann, A.; Fiore, A.; Manna, L.; Nelson, J. H.; Hill, D.; van Sark, W., Fabrication and spectroscopic studies on highly luminescent CdSe/CdS nanorod polymer composites. *Beilstein J. Nanotechnol.* **2010,** *1*, 94-100.

22. Pietra, F.; Rabouw, F. T.; van Rhee, P. G.; van Rijssel, J.; Petukhov, A. V.; Erné, B. H.; Christianen, P. C. M.; de Mello Donegá, C.; Vanmaekelbergh, D., Self-Assembled CdSe/CdS Nanorod Sheets Studied in the Bulk Suspension by Magnetic Alignment. *ACS Nano* **2014,** *8* (10), 10486-10495.

23. Yasuo Tomita, M. K., Jun-ichiro Takahashi, Jinxin Guo, Measurement of polymerizationshrinkage evolution during curing in photopolymer with a white-light Fabry-Perot interferometer. *Opt. Express* **2015,** *23* (12).

24. Li, L.-s. Anisotropy in CdSe Quantum Rods. University of California, Berkley, 2003.

25. Ameloot, M.; vandeVen, M.; Acuna, A. U.; Valeur, B., Fluorescence anisotropy measurements in solution: Methods and reference materials (IUPAC Technical Report). *Pure Appl. Chem.* **2013,** *85* (3), 589-608.